PERGAMON

Journal of Structural Geology 22 (2000) 1181–1198

JOURNAL OF STRUCTURAL GEOLOGY

www.elsevier.nl/locate/jstrugeo

Timing and duration of syn-magmatic deformation in the Mabel Downs Tonalite, northern Australia

Simon Bodorkos[a,*], Peter A. Cawood[a], Nicholas H.S. Oliver[b]

[a]*Tectonics Special Research Centre, School of Applied Geology, Curtin University of Technology, GPO Box U1987, Perth, Western Australia 6845, Australia*

[b]*Economic Geology Research Unit, School of Earth Sciences, James Cook University, Townsville, Queensland 4811, Australia*

Received 21 May 1999; accepted 31 March 2000

Abstract

Detailed outcrop mapping combined with microstructural and U–Pb SHRIMP zircon data indicate that emplacement of the Mabel Downs Tonalite spanned progressive regional D_3 deformation in the Palaeoproterozoic Halls Creek Orogen of northern Australia, and that the duration of magmatism exceeded the crystallisation time of the pluton had its entire volume been emplaced instantaneously ($\sim 10^5$ y). The pluton comprises several compositionally distinct phases, which show (i) a regional solid-state S_{3a} foliation-forming event, predated by a strongly deformed porphyritic monzogranite with a U–Pb SHRIMP zircon age of 1837.3 ± 6.0 Ma (95% confidence level); and (ii) overprinting by the localised S_{3b} Ord River Shear Zone, which crosscuts a 1831.9 ± 3.3 Ma foliated granodiorite and contains 1826.6 ± 7.3 Ma undeformed felsic veins, providing a younger age limit for D_3 deformation.

The protracted nature of deformation and magmatism during regional D_3 deformation is significant in the context of the evolution of Halls Creek Orogen, which is characterised by a prolonged thermal event spanning three regional deformation events (D_2, D_3 and D_4) within a 30–40 million-year interval. The accumulated finite strain is more probably the product of relatively long-lived events (of the order of several millions of years) with low average crustal strain rates, rather than high crustal strain rates during short-lived deformation episodes ($= 10^5$ y). Thus the partitioning of strain accumulation into discrete deformation events during the rapid development of the Halls Creek Orogen was probably not as pronounced as in orogenic belts characterised by higher accumulated strain or longer intervals between deformation events.

1. Introduction

The concept of 'syn-tectonic' intrusions has assumed critical importance in the interpretation of deformation and magmatic histories of many orogenic belts (e.g. Hutton, 1988; Karlstrom, 1989; Paterson, 1989). However, despite the common spatial and temporal association between granites and crustal-scale shear zones (e.g. Brown and Solar, 1998; Solar et al., 1998), the recognition of unambiguous indicators of synchroneity of plutonism and emplacement-level deformation is often not straightforward. The large-scale, progressive nature of many orogenic events generally results in complex regional structural signatures, including variations in the number of recognisable (overprinting) deformation events within an orogenic cycle. Even within a single regional deformation event, structural interference in the vicinity of pre-existing competent intrusive bodies may result in deformation patterns which are difficult to interpret. For example, apparent continuity in foliations from intrusions into their host rocks is to be expected, since pre-existing fabrics in a deformed host rock are likely to influence strongly the structural

* Corresponding author. Tel.: +61 8 9266 7263; fax: +61 8 9266 3153.

E-mail address: simonb@lithos.curtin.edu.au (S. Bodorkos).

0191-8141/00/$ - see front matter
PII: S0191-8141(00)00035-3

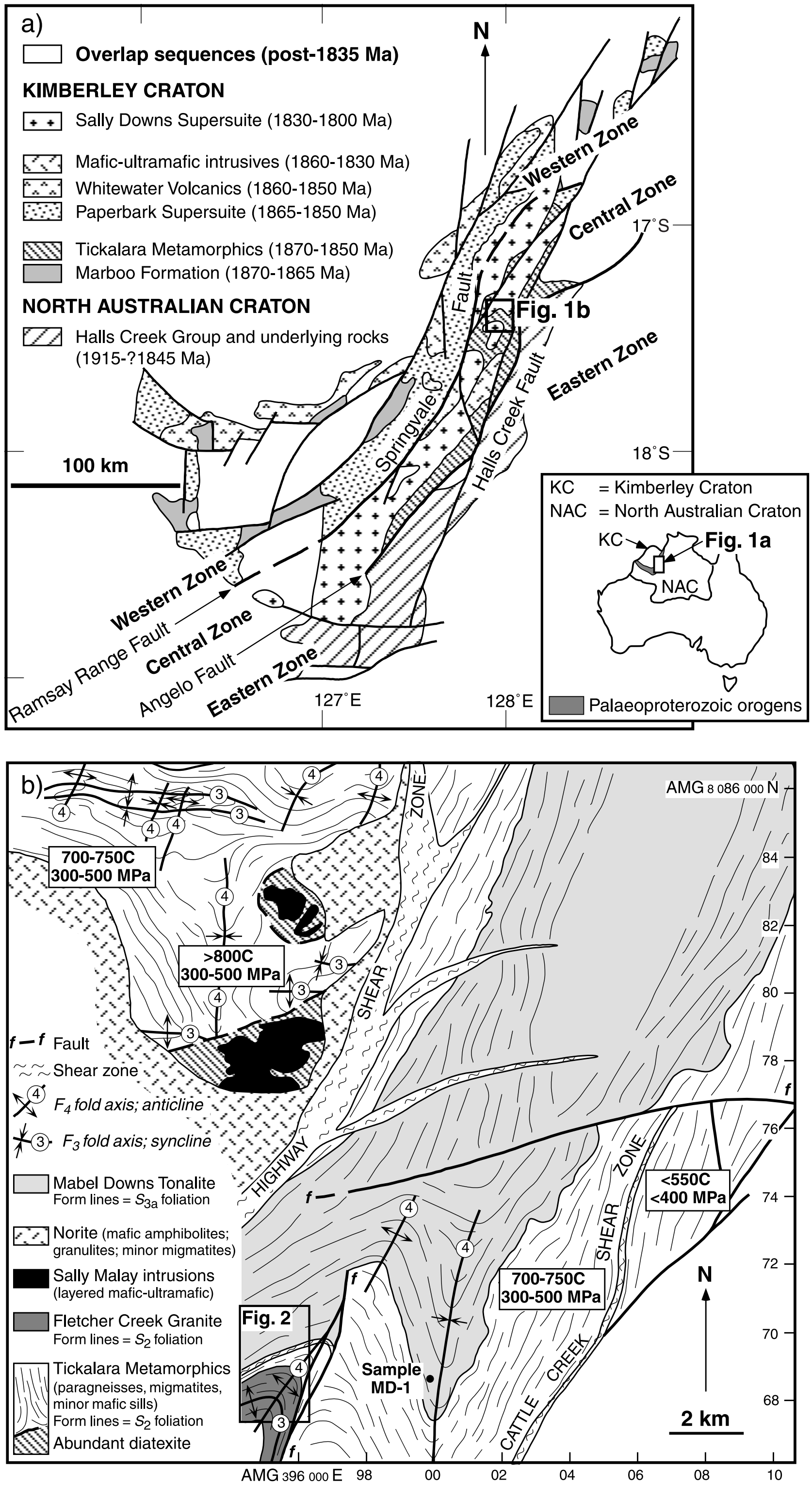

Fig. 1. (a) Map showing major lithological units comprising the Palaeoproterozoic Halls Creek Orogen (modified from Tyler et al., 1995). The Western and Central zones (separated by the Ramsay Range–Springvale fault system) represent the Kimberley craton margin, whereas the Eastern zone is part of the North Australian craton (see inset). The Angelo–Halls Creek fault system forms the interface along which the two cratons have been juxtaposed. (b) Simplified geological map showing the effects of D_3 and D_4 in the study area. The Highway and Cattle Creek Shear Zones are both D_4 features. Structural and thermobarometric data for the area west of the Highway Shear Zone are from Thornett (1986). Thermobarometric data east of the Mabel Downs Tonalite are from Magart (1994). Note the location of sample MD-1 in the southern central part of the map.

features developed in any subsequent intrusion. Furthermore, evidence from plutons containing a strong magmatic fabric suggests that foliations in the host rock can be rotated into parallelism with the pluton margin during emplacement (Buddington, 1959; Castro, 1986; Paterson et al., 1989). Importantly, the observed relationships often do not preclude the possibility of the fabric-forming event significantly post-dating both the host rocks and the intrusion (e.g. Oliver et al., 1990).

Ascribing a 'syn-tectonic' origin to a single intrusion based on its relationship to a single deformation event is often a considerable simplification, since a deformation event cannot be dated directly using a single age from a syn-tectonic intrusion, regardless of the consistency of the relative deformation–intrusion event sequence. Only the timing of igneous crystallisation can be dated directly, and the absolute timing and duration of deformation can at best only be bracketed between two closely spaced intrusive events pre- and post-dating the deformation event (Gower, 1993). Thus the study of 'syn-tectonic plutons' is better approached by constraining the timing of syn-plutonic (local) deformation within an absolute chronology provided by isotopic data from bracketing intrusives (e.g. Pearson et al., 1992; Solar et al., 1998).

The Mabel Downs Tonalite in the Palaeoproterozoic Halls Creek Orogen of northwestern Australia (Fig. 1a) presents an excellent opportunity to study the duration of, and interaction between, deformation and magma injection associated with a regional orogenic event. The thermal history of this orogenic belt is regionally well-constrained by high-quality U–Pb zircon SHRIMP data (Page and Sun, 1994; Page et al., 1995a,b; Tyler et al., 1999), which provide independent controls on the timing of the deformation event (D_3) associated with intrusion of the Mabel Downs Tonalite. Regional D_3 is bracketed by preceding regional high-grade D_2–M_2 deformation and metamorphism at ~1850–1845 Ma, and subsequent magmatism producing ~1820 Ma plutons unaffected by D_3-related solid-state deformation (Page et al., 1995b; Sheppard et al., 1995; Bodorkos et al., 1999; Oliver et al., 1999). In addition, the Mabel Downs Tonalite is well-exposed along its basal contact defined by the ductile Ord River Shear Zone, and it displays strong compositional heterogeneity across short distances, allowing relationships between intrusive phases and local deformation events to be readily established.

This paper describes field relationships from key outcrops of the Mabel Downs Tonalite within the Ord River Shear Zone, in which several easily distinguishable intrusive phases display strongly consistent relative timing relationships to local deformation events. The resulting tightly constrained deformation–intrusion chronology is further refined by U–Pb SHRIMP zircon geochronological data from three granitoid phases bracketing the deformation events. These provide absolute 'time-pins' constraining the timing of granitoid emplacement, and the duration of synchronous ductile deformation and magmatism in the middle crust within a single orogenic cycle (Bodorkos et al., 1998).

2. Geological setting

The Palaeoproterozoic (~1915–1800 Ma) Halls Creek Orogen represents the collisional interface between the Kimberley and North Australian cratons (Fig. 1a). It consists of three tectono-metamorphic zones (Western, Central and Eastern), which are based on integrated field, structural, petrological and geochronological data (Griffin and Tyler, 1992; Page et al., 1995b; Tyler et al., 1995; Bodorkos et al., 1999). The Western and Central zones (Kimberley craton margin) are characterised by rapid sedimentation, followed by high-temperature, low-pressure (HTLP) metamorphism and the emplacement of granites and large layered mafic–ultramafic intrusions in the interval ~1860–1845 Ma (Fig. 1b). Voluminous post-metamorphic granitoids of the Sally Downs Supersuite intruded the Central zone in the interval ~1835–1800 Ma (Sheppard et al., 1995, 1999), spanning the ~1820 Ma collisional event, which juxtaposed the Central zone with the undeformed passive-margin sedimentary sequences of the Eastern zone (North Australian craton margin). Basal units in a sedimentary sequence overlapping all three zones have been dated at ~1800 Ma (Tyler et al., 1995).

This study is focused on the northern Central zone, where metapelitic gneisses, migmatites, metacarbonates and mafic sills of the Tickalara Metamorphics are the oldest rocks exposed. The youngest suite of detrital zircons within this unit has been dated at ~1865 Ma (Page et al., 1995a; Bodorkos et al., 2000). Rapid deposition and burial of these sediments preceded HTLP metamorphism (D_2–M_2) at ~1845 Ma (Oliver et al., 1999; Bodorkos et al., 2000), with peak regional T = 700–750°C and $P \sim 400$ MPa (Fig. 1b). Emplacement of the Sally Malay layered mafic–ultramafic intrusion (U–Pb SHRIMP zircon age 1841 ± 3 Ma; Trudu and Hoatson, 1996) post-dated peak metamorphism, producing abundant diatexites (local T = 800°C) which cross-cut regional stromatic migmatites.

The Tickalara Metamorphics are affected by macroscopic F_3 folds, which vary in character from the north to south across the study area (Fig. 1b). F_3 folds in the north are mostly open, shallow-plunging, east–west-trending structures defining a dome and basin system (Thornett, 1986; Oliver and Barr, 1997), which is largely undisturbed by subsequent deformation. Further south, F_3 folds are tight to isoclinal and fold axis orientations vary widely, reflecting interference from macroscopic F_4 structures (Fig. 2). Emplacement of the ~1830 Ma Mabel Downs Tonalite is broadly synchronous with the D_3 event, and its southwestern contact is defined by the kilometre-scale ductile D_3 Ord River Shear Zone (Fig. 2). The pluton forms the hanging wall of this steeply northwest-dipping, locally northeast-striking dextral shear zone (Kendrick et al., 1999), which is oriented parallel to the trace of the F_3 axial surface in the Fletcher Creek Granite lying in the footwall. East of the Ord River Shear Zone, the Mabel Downs Tonalite is characterised by direct intrusive contacts with the metasedimentary host rocks.

3. Relationships between the Mabel Downs Tonalite and regional D_3

The Mabel Downs Tonalite is the largest of the plutons comprising the ~1835–1800 Ma Sally Downs Supersuite (Sheppard et al., 1995, 1997). Although the Mabel Downs Tonalite is dominated by tonalite and granodiorite, the southern part of the pluton is compositionally heterogeneous, ranging from fine-grained hornblende ± orthopyroxene diorite to coarse-grained porphyritic microcline-bearing monzogranite and pegmatitic leucocratic trondhjemite. At least six different intrusive phases are readily distinguishable in the field, although 'boundaries' between them are often imperceptibly gradational in nature.

The Mabel Downs pluton was emplaced broadly

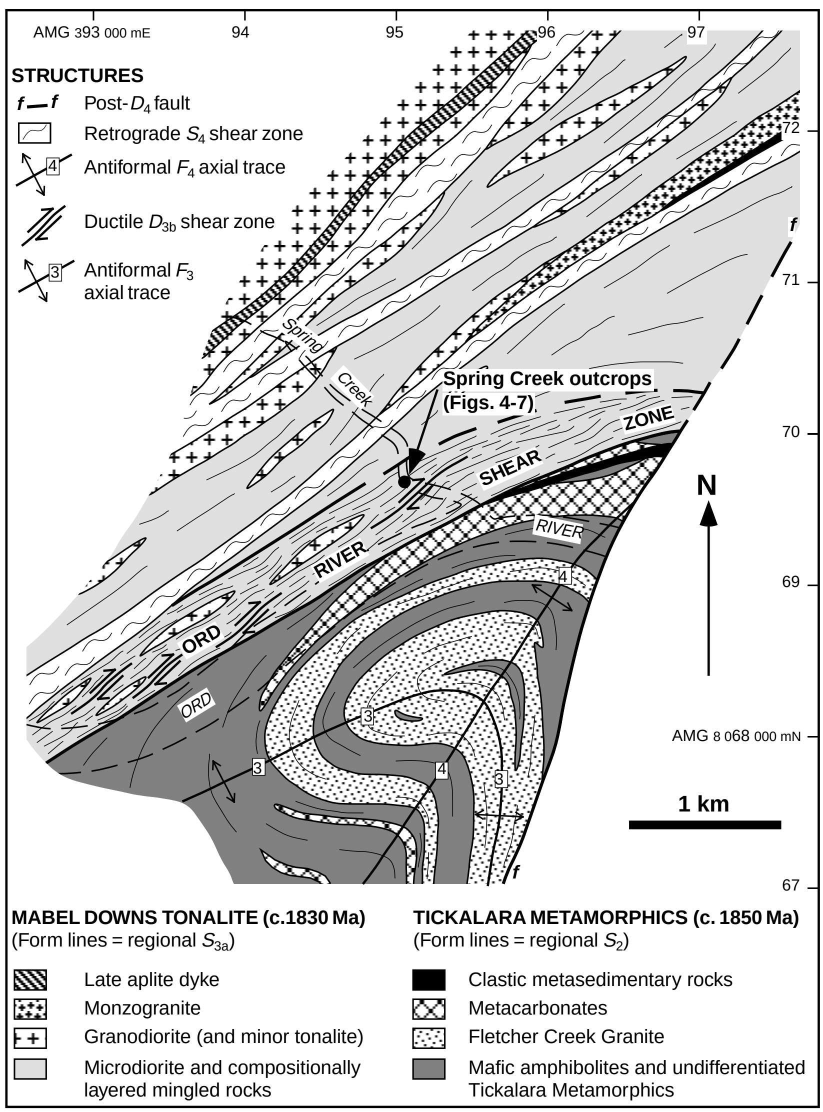

Fig. 2. Geology of the southern margin of the Mabel Downs Tonalite, which is separated from the host Tickalara Metamorphics by the steeply north-dipping ductile Ord River Shear Zone (see Fig. 1b for location). Note the F_3 antiform refolded by the F_4 antiform south of the Ord River Shear Zone, and the truncation of the northern limb of this fold by the shear zone.

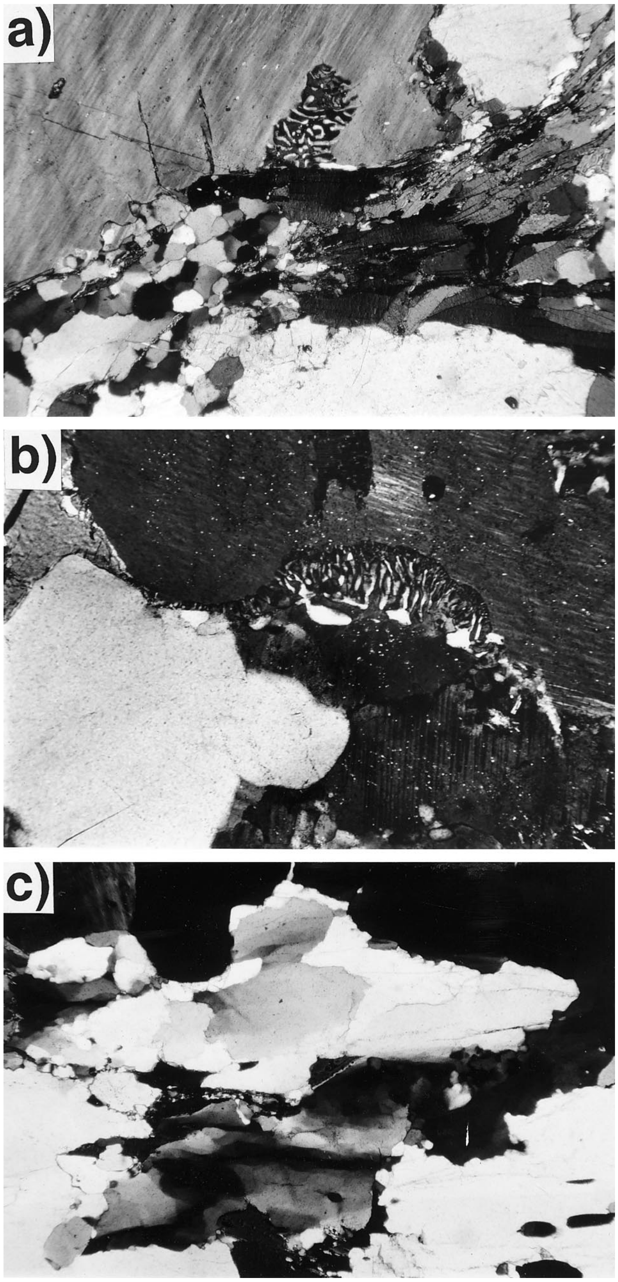

Fig. 3. Photomicrographs showing microstructural features of porphyritic monzogranite MD-1. (a) Aggregates of recrystallised quartz and semi-continuous biotite along the margin of a large microcline phenocryst (top left). Note the preservation of delicate lobes throughout the myrmekitic intergrowth embaying the microcline phenocryst, where it was shielded from the high strains along the crystal margin. Long axis of photo = 2.8 mm, crossed polars. (b) Myrmekite showing the effect of shearing along feldspar grain boundaries. Delicate lobate intergrowths are preserved along the myrmekite growth front, which embays the microcline crystal (top right). The bottom half of the myrmekite has been completely recrystallised to anhedral quartz (white patches) and plagioclase (bottom right, in extinction). Long axis of photo = 1.1 mm, crossed polars. (c) Preferred orientation of undulose extinction zones in a quartz aggregate (top centre) parallel to the long axis of the photo. This quartz aggregate is surrounded by feldspars (top left, top right, in extinction along bottom of photo). Long axis of photo = 2.8 mm, crossed polars.

synchronous with regional D_3, which locally comprises two distinguishable and sequential foliation-forming events (D_{3a} and D_{3b}). These two deformation events differ in terms of their regional extent and relationships with various intrusive phases of the Mabel Downs Tonalite. D_{3a} is evident throughout the exposure of the pluton in the study area as a foliation of varying intensity, oriented parallel to the margins of the intrusion (Fig. 1b). This S_{3a} foliation formed during regional D_3, which resulted in east–west-trending macroscopic F_3 folds in the Tickalara Metamorphics west of the D_4-related Highway Shear Zone (Fig. 1b) and south of the D_{3b} Ord River Shear Zone (Fig. 2). However, macroscopic F_3 fold closures are not present in the Mabel Downs Tonalite or the nearby Tickalara Metamorphics. Deformation related to D_{3b} is mostly confined to the immediate vicinity of the Ord River Shear Zone, which truncates the northern limb of the refolded D_{3a} fold in the Fletcher Creek Granite (Fig. 2).

Relationships between deformation and the volumetrically dominant granitoid phases are described in the context of regional D_{3a}, whereas outcrop-scale mapping and observations are used to document features of the areally restricted D_{3b} event. Three representative intrusive phases of the Mabel Downs Tonalite (porphyritic monzogranite MD-1, biotite granodiorite MD-2 and microgranodiorite MD-3), which display a range of field relationships with respect to D_{3a} and D_{3b} deformation, were targeted for microstructural study and U–Pb SHRIMP zircon dating, in order to impose further constraints on the nature and absolute chronology of D_3 deformation.

3.1. Regional D_{3a}

The S_{3a} foliation is observed in the vast majority of homogeneous granitoid phases of the Mabel Downs Tonalite, although foliation intensity increases appreciably toward the margins. In the core of the pluton, coarse-grained (~5–10 mm) foliated porphyritic light- to dark-grey tonalite is characterised by the alignment of 20–30 mm hornblende or sodic plagioclase phenocrysts in a groundmass of plagioclase, biotite and quartz. Closer to the pluton margins, light-grey porphyritic granodiorite contains a foliation defined by the alignment of plagioclase phenocrysts and/or semi-continuous biotite aggregates. Irregular lenses and sheets of pinkish-grey porphyritic monzogranite (e.g. sample MD-1; Fig. 2) occur along the southern margin of the pluton, and these rocks contain a strongly developed S_{3a} fabric defined by semi-continuous, aligned subhedral biotite grains and fine-grained quartz folia wrapping large (up to 30–40 mm) rounded phenocrysts of vitreous microcline (Fig. 3a). Groundmass plagioclase generally preserves little primary twinning, with the exception of rare small inclusions within microcline. Myrmekitic intergrowths of quartz and feldspar with curved lobes are commonly observed growing into microcline along boundaries between microcline and plagioclase grains. The presence of curved (rather than straight) lobes indicates myrmekite growth probably took place during ductile deformation along the feldspar grain boundaries (Fig. 3b, see also Vernon, 1991). Extensive recrystallisation of groundmass minerals has occurred along the edges of anhedral microcline phenocrysts, resulting in fine-grained polygonal aggregates dominated by quartz, plagioclase and minor biotite. Larger quartz grains and aggregates, which have not been pervasively recrystallised, display moderate elongation parallel to the foliation and strongly undulose extinction (Fig. 3c), with sub-grain boundaries aligned parallel to the elongation direction. These microstructural features typify granitoids close to the intrusive contacts of the Mabel Downs Tonalite, and are consistent with subsolidus fabric development (Paterson et al., 1989).

3.2. Ord River Shear Zone and D_{3b} deformation

The kilometre-scale ductile D_{3b} Ord River Shear Zone truncates the northern limb of the macroscopic F_{3a} fold in the Fletcher Creek Granite (Fig. 2), and separates the Mabel Downs Tonalite from the Tickalara Metamorphics. However, rocks in the vicinity of

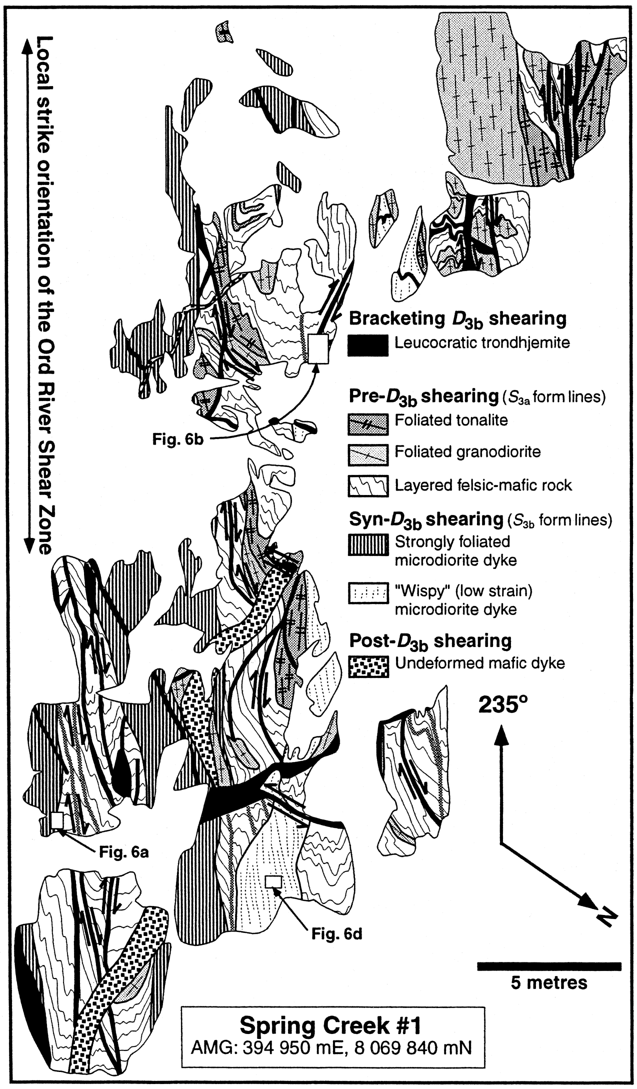

Fig. 4. Detailed map of an outcrop in Spring Creek (AMG 394900 mE, 8069850 mN) within the Ord River Shear Zone, illustrating field relationships between mappable intrusive phases and local D_{3a} and D_{3b} events (see Fig. 2 for location). Rock types are grouped on the basis of their relationship to D_{3b} shearing. Leucocratic trondhjemite is observed pre- and post-dating D_{3b}. Form lines in tonalite and granodiorite represent S_{3a} foliations, and in mafic–felsic rocks they represent S_{3a}-parallel compositional layering. The fill pattern in sheared microdiorite approximates the strong S_{3b} foliation, which is represented by thin grey lines in the 'wispy' microdiorite dyke.

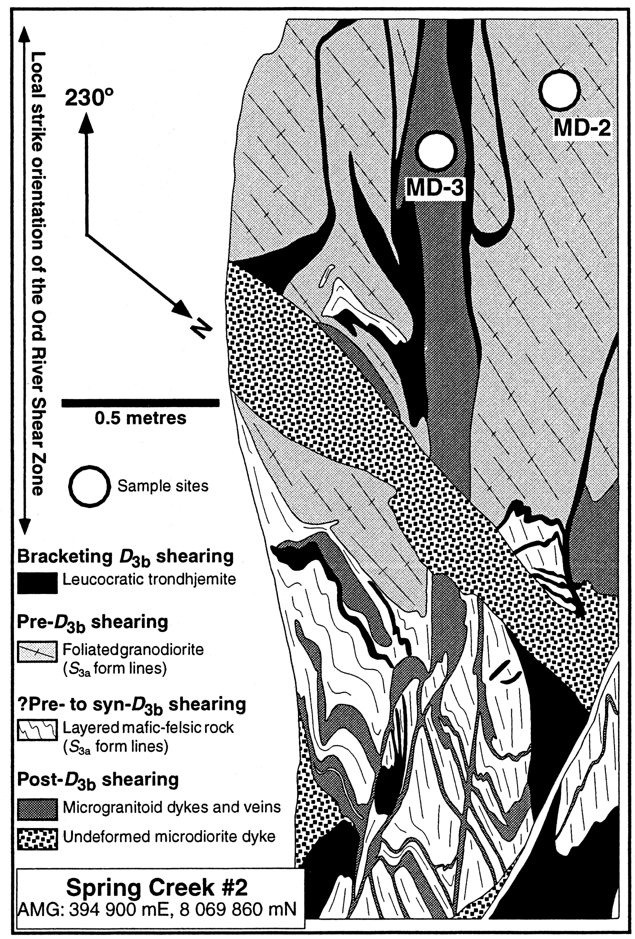

Fig. 5. Detailed map of an outcrop within ~50 m of the outcrops depicted in Fig. 4, showing the sample locations of biotite granodiorite MD-2, microgranodiorite vein MD-3 and their relationships to local D_{3a} and D_{3b} events. Form lines in granodiorite represent S_{3a} foliations, and in layered mafic–felsic rocks S_{3a}-parallel compositional layering. Form lines in microgranodiorite vein MD-3 represent a weak magmatic (late-D_{3b}?) foliation.

the Ord River Shear Zone are dominated by fine-grained hornblende–plagioclase microdiorites, which are extensively and intimately intermingled with felsic granitoids of the Mabel Downs Tonalite, at scales ranging from centimetres to hundreds of metres. Field relations suggest the existence of several distinguishable episodes of granodiorite, microdiorite and microgranite magma injection, displaying a range of relationships to regional D_{3a} and local D_{3b} deformation.

Careful mapping of outcrops in the rocky bed of Spring Creek [Australian Map Grid (AMG) 394900 mE, 8069850 mN] within the Ord River Shear Zone (Fig. 2) was undertaken in order to examine properly the local interplay between episodic magma injection and overprinting deformation. These key outcrops (Figs. 4 and 5) are well-suited to the purpose because (i) they contain several compositionally distinct and relatively easily mappable intrusive phases; (ii) the intrusive phases display consistent cross-cutting relationships; and (iii) magmatic episodes completely bracket the D_{3a}–D_{3b} interval and occupy consistent positions in the deformation chronology (Figs. 4 and 5). It is therefore convenient to describe the mapped igneous units on the basis of their relationship to the D_{3b} event.

3.2.1. Pre-D_{3b}

The oldest rocks exposed in the Ord River Shear Zone pre-date D_{3b}, and include voluminous, compositionally heterogeneous fine-grained hornblende–plagioclase microdiorites, together with lenses and irregular-shaped bodies of homogeneous granodiorite (and minor tonalite). The microdiorites feature pervasive mingling of dioritic and granitic magma during emplacement, resulting in the incorporation of significant volumes (up to 30–40 vol.%) of felsic material and the production of extensive, compositionally layered rocks (hereafter referred to as 'layered mafic–felsic rocks') with extremely regular alternations of fine-grained hornblende–plagioclase and coarser quartzo-feld-

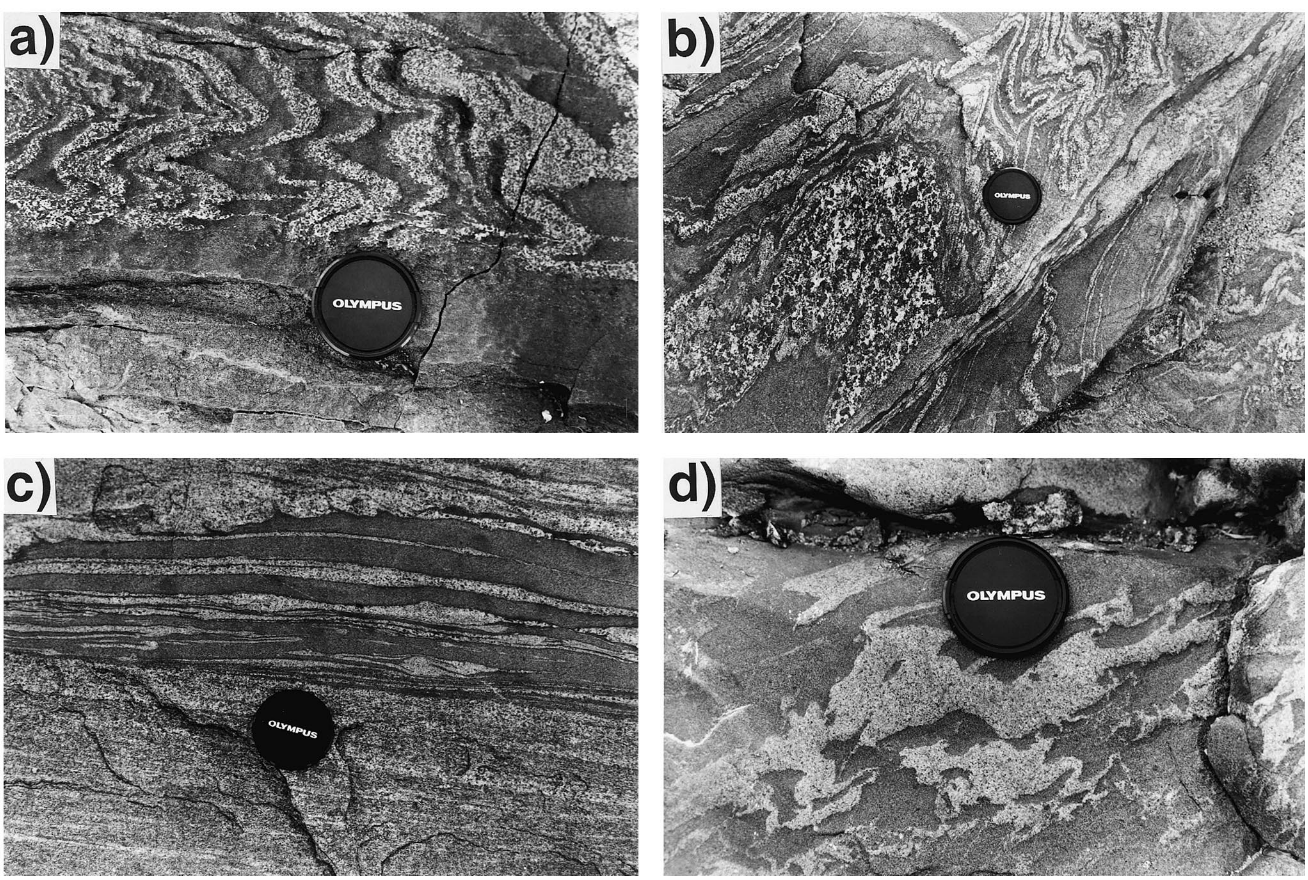

Fig. 6. Field photographs from the Spring Creek outcrops within the Ord River shear zone. The location of (a), (b) and (d) are shown on Fig. 4, and (c) is from an outcrop less then 100 m to the south of Fig. 4. Camera lens cap = 5 cm in diameter. (a) Syn-S_{3b} microdiorite dyke (lower half of photo) cross-cutting layered mafic–felsic rock. Note the compositional S_{3a} layering is folded with axial surface trace parallel to the S_{3b}-parallel dyke. (b) A thick layer of coarse-grained leucocratic trondhjemite (lower left corner of photo) lying parallel to S_{3a} layering in the host mafic–felsic rock, and pre-dating a small S_{3b} shear zone. (c) Ptygmatic rootless intrafolial folds in a microdiorite dyke intruded prior to the major S_{3b} shearing event. (d) 'Wispy' irregular patches and blobs of felsic material within a weakly foliated microdiorite dyke. This is interpreted as a low-strain version of the strongly sheared microdiorite dyke in (c), probably due to its intrusion post-dating the major S_{3b} shearing episode.

spathic layers at a 5–20 mm scale. Layering in the mafic–felsic rocks is usually S_{3a}-parallel and is commonly tightly folded, with F_{3b} axial surface traces parallel to the S_{3b} shear zones (Fig. 6a; see Fig. 4 for location).

Homogeneous granitoid phases contain an S_{3a} foliation which is often slightly oblique to, or locally rotated into parallelism with, the small (metre-scale) S_{3b} shear zones which form their boundaries (Fig. 4). They are relatively fine-grained and equigranular in comparison to monzogranite MD-1 described above, but display some textural similarities. In the equigranular granodiorite MD-2 (see Fig. 5 for location), S_{3a} is defined by continuous aggregates of aligned subhedral biotite. Undulose extinction is common in many quartz aggregates, but no significant elongation parallel to the foliation is evident, and fine-grained polygonal recrystallised aggregates are rare in comparison with monzogranite MD-1. Feldspar crystal faces are not preserved (Fig. 7a) and plagioclase grains up to 5 mm are often equant, and only slightly larger than the majority of the groundmass (~2 mm). However, plagioclase crystals with discernible long axes are oriented broadly parallel to the foliation, and remnant primary twinning is parallel to the long axes. Curvature of twinning in elongate plagioclase crystals is occasionally observed (Fig. 7a), suggesting the presence of a primary magmatic fabric in granodiorite MD-2 which is incompletely overprinted by a solid-state tectonic S_{3a} foliation. In addition, distinctive but volumetrically minor coarse-grained leucocratic trondhjemite, which comprises plagioclase (up to 50–60 mm) in a finer-grained groundmass of strained quartz, accessory biotite and magnetite, is occasionally found lying parallel to S_{3a} within layered mafic–felsic rock (Fig. 6b, see also figure 8a in Bodorkos et al., 1999).

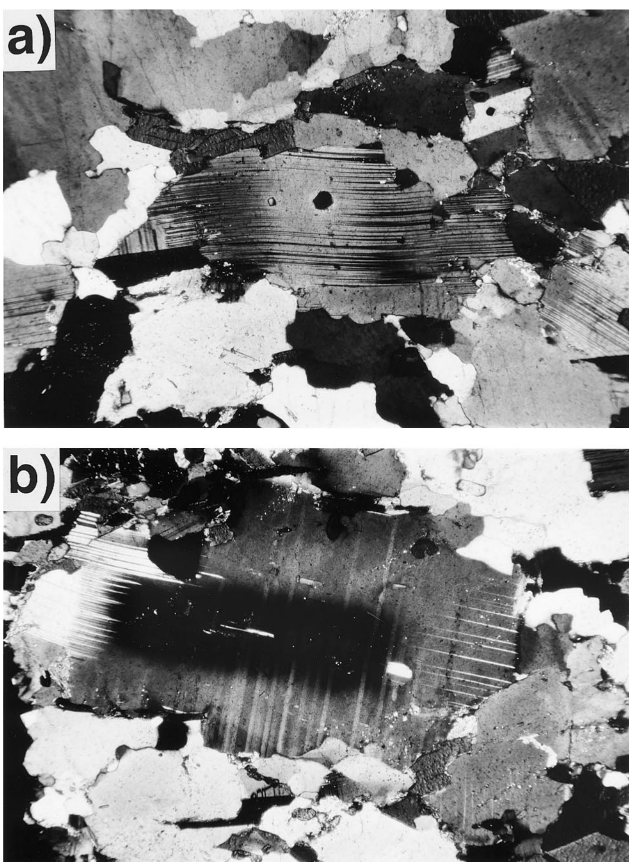

Fig. 7. Photomicrographs showing microstructural features of granitoids in the Ord River Shear Zone (see Fig. 5 for location). (a) Granodiorite MD-2. Curvature of twins in an elongate plagioclase crystal oriented parallel to the S_{3a} foliation. The lack of preservation of crystal faces and the undulose extinction present in quartz (top left) suggest that magmatic alignment of plagioclase has been overprinted by a solid-state tectonic fabric. Long axis of photo = 2.8 mm, crossed polars. (b) Microgranodiorite MD-3. Plagioclase grain retaining primary igneous features, such as compositional oscillatory zoning and long axis-parallel primary twinning. Minor recrystallisation of grain boundaries is the only evidence for subsequent solid-state deformation. Long axis of photo = 2.8 mm, crossed polars.

3.2.2. Syn-D_{3b}

Broadly northeast-trending small-scale folds and dextral ductile shear zones at a range of scales are the principal expression of D_{3b}. In the Spring Creek outcrops, S_{3b} shear zones are up to 10 m long but rarely more than a few centimetres wide (Fig. 6b, see Fig. 4 for location). Microdiorite and leucocratic trondhjemite are both commonly observed lying within the S_{3b} shear zones, and syn-S_{3b} microdiorite dykes characteristically contain a distinctly lower proportion of incorporated felsic material (rarely exceeding 10–15 vol.%) in comparison to pre-D_{3b} layered mafic–felsic rocks.

Variations in the intensity of D_{3b} deformation are evident in two adjacent S_{3b}-parallel microdiorite dykes (both 'syn-D_{3b}' in Fig. 4) which, despite having very similar compositions and proportions of incorporated felsic magma (~10 vol.%), appear to have experienced vastly different strain histories. The 'strongly foliated' southwestern dyke (see Fig. 4 for location) contains a very strong S_{3b} foliation, reflected by isoclinal rootless intrafolial folds in the felsic veinlets, with thickened hinges and occasionally ptygmatic style. Similar features in a microdiorite dyke from a nearby outcrop are shown in Fig. 6(c) (see also figure 8b in Bodorkos et al., 1999). In contrast, the 'wispy' northeastern dyke (see position of Fig. 6d in Fig. 4 for location) contains only a very weak foliation, and the felsic material occurs as irregular patches and blobs (Fig. 6d, see Fig. 4 for location). These 'wispy' mingled rocks are interpreted as low-strain equivalents of the sheared microdiorites containing strongly deformed felsic veinlets.

The observed strain and deformation patterns observed in the microdiorite dykes can be explained by (i) an age difference, in which the S_{3b}-parallel dykes bracket and are broadly synchronous with D_{3b}, or (ii) heterogeneity in strain distribution. In outcrop, D_{3b} strain is preferentially partitioned into microdiorite dykes at all scales, the vast majority of which are strongly sheared in comparison with the older granitoids. Heterogeneous strain distribution is observable within a nearby single microdiorite dyke less than 50 cm in thickness (figure 8c in Bodorkos et al., 1999), and while it is possible that the 'wispy' microdiorite dyke was protected from D_{3b} shearing in a low-strain zone tens of metres wide, we consider it more likely that intrusion post-dated the majority of S_{3b} shearing.

3.2.3. Post-D_{3b}

Several undeformed intrusive phases post-date D_{3b}. Fine-grained equigranular felsic veins up to 30 cm in width with diffuse boundaries cross-cut S_{3a}-bearing granitoids (Fig. 5), and although they are commonly subparallel to S_{3b}, they preserve only a very weak foliation. Microgranodiorite MD-3 was collected from one such vein (Fig. 5), and it features well-preserved plagioclase crystals with igneous microstructures such as oscillatory (compositional) zoning and twinning parallel to feldspar long axes (Fig. 7b). Rare biotite is randomly oriented, and undulose extinction is only occasionally observed in quartz. These microstructures are interpreted as a weak magmatic fabric developed during vein injection, and there is no evidence for overprinting solid-state deformation. Homogeneous undeformed mafic dykes (Figs. 4 and 5) cross-cut all units, and are distinguished from pre- and syn-D_{3b} microdiorite dykes on the basis of their finer grain size and the absence of incorporated felsic veinlets.

4. Zircons and U–Pb SHRIMP data

Zircons from samples MD-1, MD-2 and MD-3 were analysed using the Sensitive High-Mass Resolution Ion Micro Probe (SHRIMP), in order to place constraints on the timing of syn-magmatic deformation associated with regional D_3. Porphyritic monzogranite MD-1 contains a strong solid-state S_{3a} fabric, and its igneous crystallisation age provides an older age limit for pluton-scale D_{3a} deformation. Equigranular biotite granodiorite MD-2 contains an S_{3a} foliation truncated by an S_{3b} shear zone (Fig. 6), and imposes an older age limit on D_{3b} shearing. Directly cross-cutting granodiorite MD-2, leucocratic microgranodiorite MD-3 is a felsic vein ~10 cm wide subparallel to S_{3b}, which does not contain any evidence of ductile deformation, and either post-dates or was intruded during the very latest stages of D_{3b}.

Zircon crystals were extracted from each sample via standard crushing, heavy liquid separation, sieving and magnetic separation techniques. These grains were mounted in epoxy, along with fragments of the laboratory U–Pb standard (zircon CZ3 from Sri Lanka = 564 Ma), and polished to half their thickness prior to gold-coating. The mount was photographed in transmitted and reflected light, before cathodoluminescence (CL) imaging of the zircon grains was carried out using a JEOL 6400R scanning electron microscope at the University of Western Australia, with an accelerating voltage of 15 kV and a beam current of 1–3 nA.

Selected grains were then analysed using the SHRIMP II at Curtin University. Procedures, operating conditions for the instrument and data reduction techniques are detailed in Nelson (1997), and briefly summarised here. Targeted grains were sputtered using

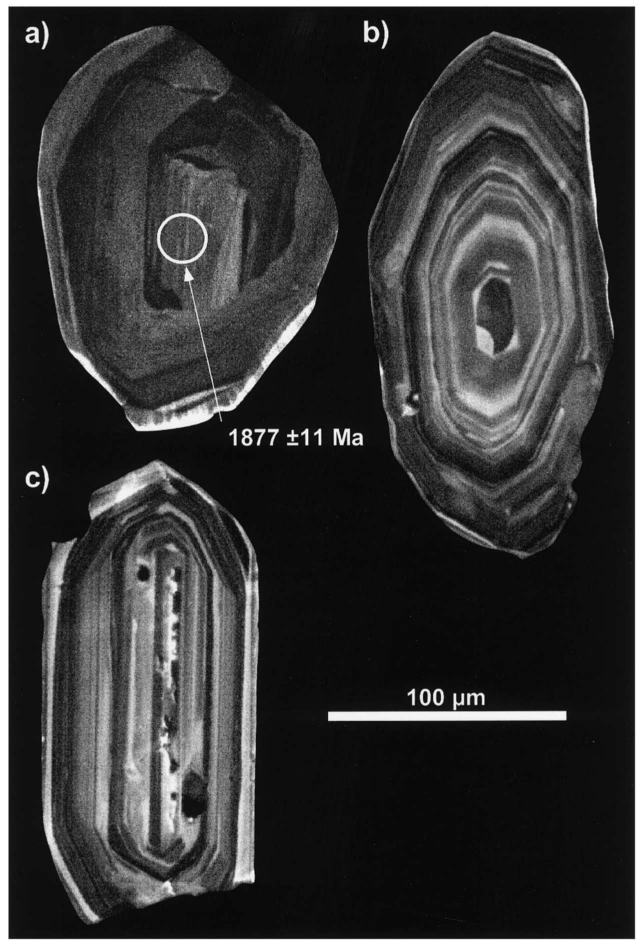

Fig. 8. Cathodoluminescence (CL) images of zircons from intrusive phases of the Mabel Downs Tonalite. (a) Low-U zircon from porphyritic monzogranite MD-1, showing an inherited core surrounded by broad, poorly defined growth zoning. The white circle represents the location of the ion probe spot (~25 µm diameter), and the ^{204}Pb -corrected $^{207}Pb/^{206}Pb$ age ($\pm 1\sigma$ error) of the intragrain analysis is shown. (b) Prominent concentric oscillatory zoned zircon from granodiorite MD-2, illustrating the effect of the shape of the zircon 'seed' on the external morphology of the crystal. (c) Concentric oscillatory-zoned zircon from granodiorite MD-2, with a needle-shaped core. The slightly patchy CL emission of the central region probably reflects lattice defects resulting from a very rapid initial stage of zircon growth.

an O_2^- primary beam and a spot size with a diameter of approximately 20 μm. Sequential measurements of the $^{196}Zr_2O^+$, $^{204}Pb^+$, background, $^{206}Pb^+$, $^{207}Pb^+$, $^{208}Pb^+$, $^{238}U^+$, $^{248}ThO^+$ and $^{254}UO^+$ peaks in the secondary ion beam were made using an electron multiplier in pulse counting mode. Common Pb corrections were made using Broken Hill Pb isotopic compositions because $^{204}Pb^+$ counts in the standard CZ3 zircon and the unknowns were very similar. Inter-element bias in the Pb/U isotopic ratios were corrected using a linear calibration of $^{206}Pb^+/^{238}U^+$ vs. $^{254}UO^+/^{238}U^+$ for the U–Pb standard CZ3 zircon. ^{204}Pb-corrected $^{207}Pb/^{206}Pb$ ratios and ages for individual SHRIMP spots are reported with 1σ analytical errors, which include external errors of $\pm 1.45\%$ (sample MD-1, Table 1), $\pm 1.73\%$ (sample MD-2, Table 2) and $\pm 1.58\%$ (sample MD-3, Table 3) associated with the calibration of Pb/U ratios in the standard CZ3 zircon. Errors on weighted mean ages are at the 95% confidence level unless otherwise indicated.

4.1. Monzogranite MD-1

Zircons from monzogranite MD-1 are mostly subhedral and clear to light brown in transmitted light. Most grains have aspect (length/width) ratios of approximately 2:1, ranging up to 4:1 and 400 μm in length. They are characterised by low U contents (< 200 ppm), and internal structures are difficult to decipher using SEM imaging due to their low cathodoluminescence (CL) emission. The outer parts of most grains are characterised by broad, ill-defined growth zones (e.g. Fig. 8a) overgrowing a low-CL core, the shape of which governs the external morphology of the crystal. One of the analysed zircons (Fig. 8a) contains a xenocrystic core with anomalously high CL emission.

A total of 30 analyses were performed on zircons from monzogranite MD–1 (Table 1) and results are presented in Fig. 9(a). Analysis MD1–14, which sampled the xenocrystic core (Fig. 8a), was excluded

Table 1
Results of 30 ion microprobe analyses from foliated (pre-D_{3a}) porphyritic monzogranite MD-1. All errors are $\pm 1\sigma$. Common ^{206}Pb(%) is a measure of the amount of common ^{206}Pb as a percentage of the total measured ^{206}Pb at each spot, assuming Broken Hill isotopic Pb compositions

Spot	U (ppm)	Th (ppm)	Th/U	Common ^{206}Pb(%)	$^{206}Pb^a/^{238}U$	$^{207}Pb^a/^{235}U$	$^{207}Pb^a/^{206}Pb^a$	$^{207}Pb/^{206}Pb$ age (Ma)
MD1–1	127	52	0.41	0.45	0.3253 ± 55	5.03 ± 0.12	0.1122 ± 17	1835 ± 27
MD1–2	351	193	0.55	0.14	0.3310 ± 51	5.10 ± 0.09	0.1117 ± 7	1827 ± 12
MD1–3a	429	176	0.41	0.29	0.3214 ± 49	5.02 ± 0.09	0.1132 ± 8	1851 ± 12
MD1–3b	173	67	0.39	0.24	0.3266 ± 54	5.09 ± 0.11	0.1129 ± 13	1847 ± 21
MD1–4	235	107	0.46	0.49	0.3309 ± 53	5.12 ± 0.10	0.1122 ± 12	1835 ± 19
MD1–5	178	84	0.47	0.05	0.3276 ± 53	5.09 ± 0.10	0.1127 ± 11	1844 ± 18
MD1–6	195	104	0.54	0.34	0.3260 ± 53	5.05 ± 0.10	0.1124 ± 11	1839 ± 18
MD1–9	130	56	0.43	0.42	0.3216 ± 55	5.08 ± 0.11	0.1145 ± 15	1872 ± 23
MD1–10	180	92	0.51	0.33	0.3278 ± 54	5.08 ± 0.11	0.1123 ± 12	1837 ± 20
MD1–11	181	98	0.54	0.28	0.3301 ± 55	5.11 ± 0.11	0.1123 ± 12	1836 ± 19
MD1–12	140	60	0.43	0.26	0.3232 ± 55	5.05 ± 0.12	0.1134 ± 15	1855 ± 24
MD1–13a	149	62	0.42	0.28	0.3241 ± 55	5.01 ± 0.12	0.1121 ± 16	1834 ± 25
MD1–13b	729	151	0.21	0.18	0.3294 ± 49	5.07 ± 0.08	0.1116 ± 5	1826 ± 9
MD1–15	197	81	0.41	0.27	0.3288 ± 54	5.15 ± 0.11	0.1136 ± 13	1858 ± 20
MD1–16	475	48	0.10	0.20	0.3229 ± 49	5.01 ± 0.09	0.1124 ± 7	1839 ± 11
MD1–17	501	50	0.10	0.15	0.3333 ± 51	5.18 ± 0.09	0.1128 ± 6	1845 ± 10
MD1–18	170	80	0.47	1.59	0.3293 ± 55	4.92 ± 0.13	0.1083 ± 21	1772 ± 36
MD1–19	197	101	0.51	0.52	0.3213 ± 53	4.80 ± 0.11	0.1084 ± 15	1772 ± 25
MD1–20	186	84	0.45	0.32	0.3243 ± 54	5.13 ± 0.11	0.1147 ± 14	1876 ± 22
MD1–21	233	111	0.47	0.81	0.3316 ± 54	5.11 ± 0.11	0.1118 ± 14	1829 ± 23
MD1–22a	665	124	0.19	0.33	0.3336 ± 50	5.15 ± 0.09	0.1120 ± 6	1832 ± 10
MD1–22b	277	76	0.28	0.46	0.3354 ± 53	5.12 ± 0.10	0.1106 ± 11	1810 ± 18
MD1–23	179	75	0.42	0.39	0.3277 ± 54	5.09 ± 0.11	0.1127 ± 14	1843 ± 22
MD1–24	216	74	0.34	0.57	0.3277 ± 54	5.06 ± 0.11	0.1120 ± 14	1832 ± 22
MD1–25a	521	266	0.51	0.08	0.3300 ± 50	5.15 ± 0.09	0.1132 ± 6	1851 ± 10
MD1–25b	304	107	0.35	0.22	0.3329 ± 53	5.18 ± 0.10	0.1128 ± 10	1845 ± 15
MD1–26	454	280	0.62	0.16	0.3333 ± 51	5.16 ± 0.09	0.1122 ± 7	1836 ± 11
MD1–27	107	59	0.55	1.05	0.3333 ± 61	5.16 ± 0.16	0.1124 ± 25	1838 ± 40
MD1–28	156	67	0.43	0.65	0.3296 ± 56	5.05 ± 0.12	0.1110 ± 17	1817 ± 28
Older (pre-1850 Ma) inherited core								
MD1–14	471	172	0.37	0.14	0.3318 ± 51	5.25 ± 0.09	0.1148 ± 7	1877 ± 11

[a] Corrected for ^{204}Pb.

from subsequent calculations, and the remaining 29 analyses define a single population with a weighted mean $^{207}Pb/^{206}Pb$ age of 1837.3 ± 6.0 Ma (chi-squared = 0.97). This is interpreted as the magmatic crystallisation age, and constitutes an older age limit on the development of the solid-state S_{3a} foliation.

4.2. Granodiorite MD-2

Zircons from granodiorite MD-2 are clear to light-brown in transmitted light, similar to those from monzogranite MD-1. The grains are mostly euhedral, rarely exceed 300 μm in length, and have an average aspect ratio of approximately 3:1. U contents range up to 1000 ppm, and Th/U ratios are ~0.5. The grains show little variation in internal CL structure, with prominent concentric oscillatory zoning extending from the centres to the edges. External morphology of the zircon crystals are mostly controlled by the shape of the early-crystallised zircon 'seed' (Fig. 8b). Several grains display CL evidence for an initial stage of dendritic or needle-shaped growth (Fig. 8c), which provides insights into the conditions of zircon crystallisation. Similar patterns observed in zircons from Mesozoic intermediate plutonic rocks of the Ivrea Zone (southern European Alps) are thought to reflect low Zr diffusivity during low-temperature nucleation and growth of zircon in a water-saturated magma (G. Vavra, personal communication, 1999). Importantly, the presence of inherited or xenocrystic zircon precludes the development of dendritic or needle-shaped internal structures in magmatic zircon (G. Vavra, personal communication, 1999), confirming the absence of inherited zircon cores observed in granodiorite MD-2.

A total of 32 analyses were carried out on zircons from granodiorite MD-2 (Table 2, Fig. 9b), and these form a statistically valid single population with a weighted mean $^{207}Pb/^{206}Pb$ age of 1831.9 ± 3.3 Ma (chi-squared = 0.93). This age is identical to that

Table 2
Results of 32 ion microprobe analyses from foliated (pre-D_{3a}) biotite granodiorite MD-2. All errors are ±1σ. Common ^{206}Pb(%) is a measure of the amount of common ^{206}Pb as a percentage of the total measured ^{206}Pb at each spot, assuming Broken Hill isotopic Pb compositions

Spot	U (ppm)	Th (ppm)	Th/U	Common ^{206}Pb(%)	$^{206}Pb^{a}/^{238}U$	$^{207}Pb^{a}/^{235}U$	$^{207}Pb^{a}/^{206}Pb^{a}$	$^{207}Pb/^{206}Pb$ age (Ma)
MD2–1a	305	165	0.54	0.04	0.3286 ± 59	5.11 ± 0.10	0.1128 ± 7	1846 ± 11
MD2–1b	321	184	0.57	0.04	0.3341 ± 60	5.13 ± 0.10	0.1114 ± 6	1823 ± 10
MD2–1c	240	70	0.29	0.20	0.3330 ± 61	5.04 ± 0.10	0.1097 ± 8	1795 ± 13
MD2–2	308	140	0.46	0.08	0.3329 ± 60	5.13 ± 0.10	0.1117 ± 7	1828 ± 12
MD2–3	444	309	0.70	0.31	0.3117 ± 56	4.78 ± 0.10	0.1112 ± 8	1819 ± 13
MD2–4	167	80	0.48	0.17	0.3288 ± 61	5.05 ± 0.11	0.1114 ± 10	1823 ± 17
MD2–5	401	211	0.53	0.02	0.3062 ± 55	4.75 ± 0.09	0.1124 ± 6	1839 ± 9
MD2–6a	351	71	0.20	0.06	0.3280 ± 59	5.12 ± 0.10	0.1131 ± 6	1850 ± 9
MD2–6b	431	181	0.42	0.09	0.3363 ± 60	5.19 ± 0.10	0.1120 ± 5	1832 ± 8
MD2–7a	149	95	0.63	0.22	0.3304 ± 62	5.09 ± 0.12	0.1117 ± 12	1827 ± 20
MD2–8a	145	83	0.57	0.17	0.3268 ± 61	5.09 ± 0.11	0.1130 ± 11	1848 ± 17
MD2–8b	331	162	0.49	0.13	0.3201 ± 58	4.93 ± 0.10	0.1117 ± 7	1827 ± 12
MD2–9	232	120	0.52	0.14	0.3240 ± 59	5.03 ± 0.10	0.1127 ± 8	1843 ± 13
MD2–11	245	126	0.51	0.11	0.3297 ± 60	5.07 ± 0.10	0.1114 ± 8	1823 ± 12
MD2–12	490	304	0.62	0.02	0.3364 ± 60	5.22 ± 0.10	0.1126 ± 5	1842 ± 8
MD2–13	460	132	0.29	0.06	0.3249 ± 58	5.00 ± 0.09	0.1116 ± 5	1825 ± 8
MD2–14	905	1104	1.22	0.01	0.3315 ± 58	5.12 ± 0.09	0.1121 ± 3	1834 ± 6
MD2–15	304	159	0.52	0.02	0.3013 ± 54	4.66 ± 0.09	0.1122 ± 6	1836 ± 10
MD2–16	420	304	0.72	0.02	0.3388 ± 60	5.23 ± 0.10	0.1120 ± 5	1831 ± 8
MD2–17	194	111	0.57	0.05	0.3288 ± 61	5.05 ± 0.11	0.1115 ± 9	1824 ± 15
MD2–18	183	116	0.63	0.19	0.3282 ± 60	5.07 ± 0.11	0.1121 ± 9	1834 ± 15
MD2–19	209	86	0.41	0.19	0.3376 ± 61	5.14 ± 0.11	0.1104 ± 9	1806 ± 14
MD2–20	388	199	0.51	0.04	0.3415 ± 61	5.29 ± 0.10	0.1123 ± 5	1837 ± 8
MD2–21	426	275	0.65	0.08	0.3080 ± 55	4.74 ± 0.09	0.1117 ± 5	1827 ± 8
MD2–22	303	182	0.60	0.09	0.3411 ± 61	5.26 ± 0.10	0.1117 ± 6	1828 ± 10
MD2–23	241	168	0.70	0.06	0.3357 ± 61	5.19 ± 0.10	0.1121 ± 7	1834 ± 12
MD2–24a	941	875	0.93	0.04	0.3321 ± 58	5.12 ± 0.09	0.1119 ± 3	1831 ± 5
MD2–24b	482	280	0.58	0.11	0.3286 ± 58	5.08 ± 0.10	0.1120 ± 5	1832 ± 8
MD2–25	515	433	0.84	0.13	0.3257 ± 58	5.00 ± 0.09	0.1113 ± 6	1821 ± 9
MD2–26	443	362	0.82	0.06	0.3279 ± 58	5.08 ± 0.10	0.1123 ± 5	1837 ± 8
MD2–28	392	183	0.47	0.06	0.3381 ± 60	5.22 ± 0.10	0.1119 ± 5	1830 ± 9
MD2–29	901	576	0.64	0.01	0.3312 ± 58	5.13 ± 0.09	0.1123 ± 3	1837 ± 5

[a] Corrected for ^{204}Pb.

obtained from the homogeneous Mabel Downs Tonalite ~40 km to the northeast (1832 ± 3 Ma; Page et al., 1995b) and places an older age limit on the development of S_{3b}-parallel shear zones (Fig. 5). However, granodiorite MD-2 contains a relatively weak S_{3a} fabric in comparison to monzogranite MD-1.

4.3. Microgranodiorite MD-3

In comparison with samples MD-1 and MD-2, fewer zircons were extracted from microgranodiorite MD-3, due to its leucocratic composition and the relatively small size (< 0.5 kg) of the sample. The grains are subhedral, and mostly clear and colourless in transmitted light. Aspect ratios range from 2:1 to 3:1, and grains rarely exceed 150 μm in length. U contents are mostly in the range 100–800 ppm, and Th/U ratios are 0.1–0.8.

A total of 15 analyses were made on zircons from microgranodiorite MD-3 (Table 3, Fig. 9c). Two of these (MD3-5 and MD3-9) returned intragrain $^{207}Pb/^{206}Pb$ ages of 1908 ± 16 Ma and 1866 ± 7 Ma (1σ errors), respectively. These ages are similar to those obtained from detrital zircons in nearby metasedimentary rocks (Bodorkos et al., 2000) and are interpreted as xenocrysts rafted off the metasedimentary host rocks during magma ascent. One of the remaining 13 analyses (MD3-4b) returned a reverse discordant $^{207}Pb/^{206}Pb$ age of 1786 ± 6 Ma (1σ error), which is outside 1σ error of any other intragrain analysis (Fig. 9c). It is likely that the U–Pb isotopic system within this grain was disturbed subsequent to magmatic crystallisation, and we exclude it from further consideration.

The other 12 analyses are mostly concordant and have a weighted mean $^{207}Pb/^{206}Pb$ age of 1826.6 ± 7.3 Ma (chi-squared = 1.66). The chi-squared value suggests that the scatter observed in this small population is within the limits imposed by analytical uncertainty. This magmatic crystallisation age provides a younger age limit on the timing of D_{3b} deformation in the Ord River Shear Zone, since microgranodiorite MD-3 contains no evidence of a tectonic foliation.

4.4. Analysis and interpretation of U–Pb SHRIMP zircon data

The dating of temporally closely spaced intrusive phases via U–Pb SHRIMP zircon geochronology is complicated by the fact that errors attributable to analytical uncertainty will not only substantially exceed the total duration of the zircon-forming event, but also have considerable potential to exceed the real duration of quiescent periods between magma injection episodes. Errors at the 95% confidence level on the weighted mean ages presented above range from ±3.3 to ±7.3 Ma, and these errors probably exceed the real age differences between the granitoid phases. Nevertheless, important constraints may be imposed on the duration of magmatism and syn-plutonic deformation in the Mabel Downs Tonalite by evaluating the extent to which the three weighted mean ages presented above are distinguishable.

Fig. 10 shows the three weighted mean U–Pb SHRIMP ages plotted in probability space, assuming a

Table 3
Results of 15 ion microprobe analyses from post-D_{3b} microgranodiorite MD-3. All errors are ±1σ. Common ^{206}Pb(%) is a measure of the amount of common ^{206}Pb as a percentage of the total measured ^{206}Pb at each spot, assuming Broken Hill isotopic Pb compositions

Spot	U (ppm)	Th (ppm)	Th/U	Common ^{206}Pb(%)	$^{206}Pb^a/^{238}U$	$^{207}Pb^a/^{235}U$	$^{207}Pb^a/^{206}Pb^a$	$^{207}Pb/^{206}Pb$ age (Ma)
MD3–1a	406	56	0.14	0.05	0.3409 ± 55	5.25 ± 0.09	0.1118 ± 3	1828 ± 5
MD3–1b	423	71	0.17	0.07	0.3186 ± 51	4.94 ± 0.08	0.1125 ± 3	1840 ± 5
MD3–2a	149	117	0.78	0.05	0.3375 ± 55	5.23 ± 0.09	0.1124 ± 6	1839 ± 10
MD3–2b	310	177	0.57	0.22	0.3241 ± 54	4.95 ± 0.09	0.1108 ± 6	1813 ± 10
MD3–3a	248	189	0.76	0.26	0.3271 ± 55	5.06 ± 0.10	0.1121 ± 8	1834 ± 13
MD3–3b	815	107	0.13	0.15	0.3286 ± 53	5.02 ± 0.08	0.1107 ± 4	1811 ± 6
MD3–4a	188	122	0.65	0.34	0.3318 ± 56	5.13 ± 0.10	0.1122 ± 9	1835 ± 14
MD3–4b[b]	617	63	0.10	0.12	0.3295 ± 53	4.96 ± 0.08	0.1092 ± 4	1786 ± 6
MD3–6a	161	69	0.43	0.35	0.3073 ± 52	4.72 ± 0.10	0.1113 ± 10	1821 ± 17
MD3–7a	161	66	0.41	0.38	0.3354 ± 57	5.17 ± 0.11	0.1117 ± 10	1827 ± 17
MD3–8	420	253	0.60	0.28	0.3299 ± 54	5.05 ± 0.09	0.1111 ± 6	1818 ± 9
MD3–10	306	204	0.67	0.18	0.3342 ± 55	5.15 ± 0.09	0.1118 ± 6	1829 ± 10
MD3–11	149	73	0.49	0.25	0.3126 ± 54	4.77 ± 0.10	0.1107 ± 9	1810 ± 16
Older (pre-1850 Ma) xenocrysts								
MD3–9	595	431	0.72	0.09	0.3277 ± 53	5.16 ± 0.09	0.1141 ± 4	1866 ± 7
MD3–5	158	87	0.55	0.40	0.3126 ± 53	5.03 ± 0.10	0.1168 ± 10	1908 ± 16

[a] Corrected for ^{204}Pb.

[b] Reverse discordant analysis excluded from the calculation of the weighted mean age.

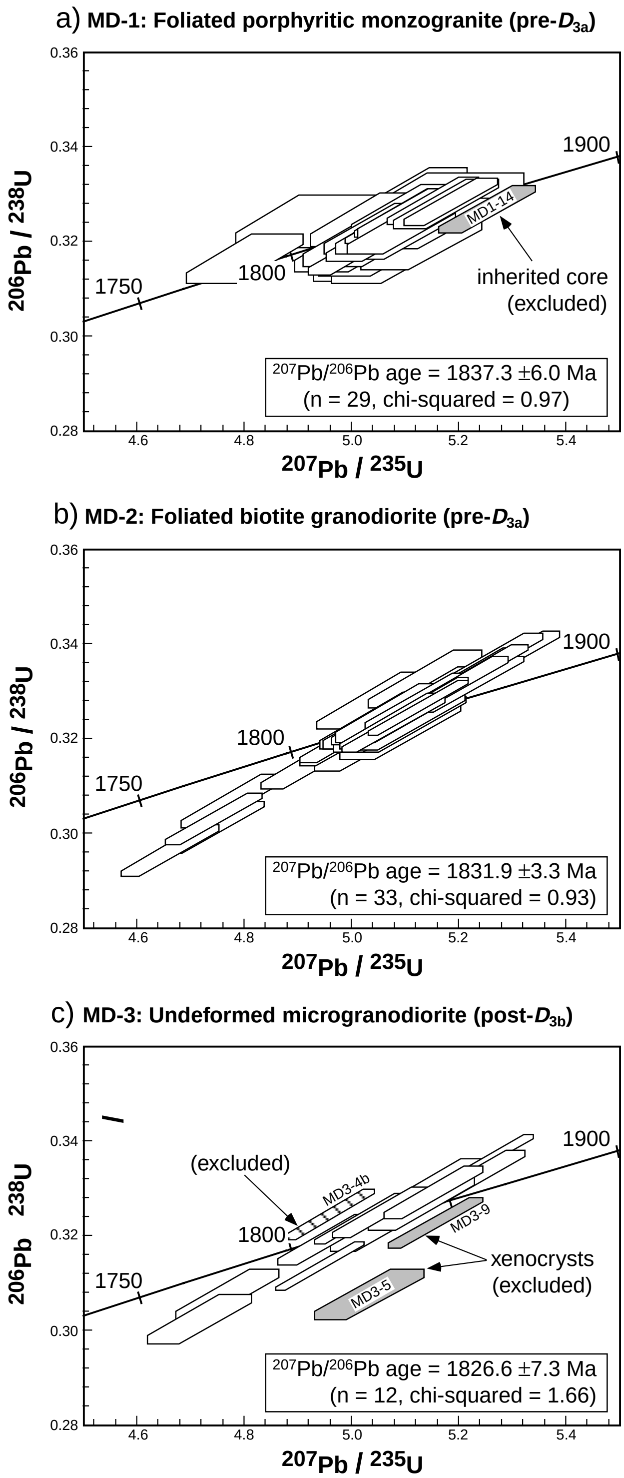

Fig. 9. Concordia plots of $^{207}Pb/^{206}Pb$ ages (corrected for ^{204}Pb). Uncertainties on individual analyses are $\pm 1\sigma$, and on pooled weighted mean ages are at the 95% confidence level.

Gaussian error distribution. The degree of distinguishability between any two of the three ages can be calculated by evaluating the probability at which the two curves intersect. These intersection points are marked on Fig. 10 with small white circles, and labelled with the two relevant sample numbers. Horizontal lines and shaded areas represent confidence level 'contours' at which each pair of ages is significantly different. For example, all three ages are distinct at the 75% confidence level, since none of the three curves intersect above this level in probability space. However, at the 95% confidence level, neither monzogranite MD-1 nor microgranodiorite MD-3 are significantly different in age from granodiorite MD-2. Nevertheless, this does not mean that all three samples are indistinguishable in age, since the age of monzogranite MD-1 remains significantly different to that of microgranodiorite MD-3 at the 95% confidence level. That these ages are significantly different at the 95% confidence level, despite the fact that errors associated with each pooled age are of the order of 6–7 million years, strongly

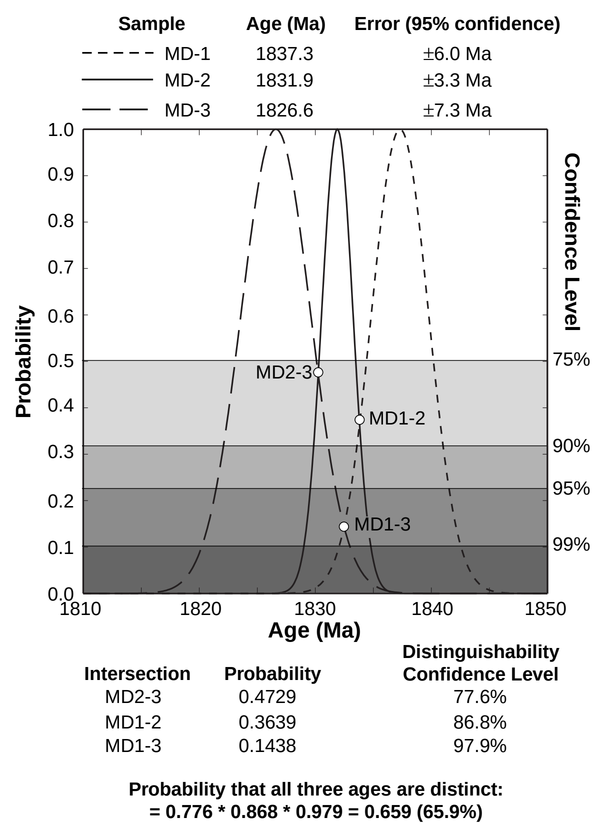

Fig. 10. Age vs. probability plot for the three weighted mean U–Pb SHRIMP ages presented in Fig. 9, assuming a Gaussian error distribution. The confidence level at which any pair of these ages are distinguishable may be calculated by evaluating the probability at which the two curves intersect (marked by small white circles, and labelled with the two relevant sample numbers). These probabilities (and the confidence levels below which each pair of ages is distinguishable) are summarised below the plot. The horizontal lines and shaded areas represent 'contours' of confidence level at which any pair of ages are significantly different. For example, all three ages are distinct at the 75% confidence level, since none of the three curves intersect above this level in probability space. However, at the 95% confidence level, MD-1 is different from MD-3 but neither may be distinguished from MD-2.

suggests that the difference in ages is attributable to some source other than analytical uncertainty, and that the total duration of magmatism during the D_3 event was of the order of several million years rather than several hundred thousand years.

The equations for each pair of curves were solved simultaneously to obtain the probability at which each pair of ages is indistinguishable. For example, the curves for MD-2 and MD-3 intersect at 1830.25 Ma, at a probability of 0.4729. Thus the probability that the MD-3 age is *older* than 1830.25 Ma is 0.4729, the probability that the MD-2 age is *younger* than 1830.25 Ma is 0.4729, and the probability that the two ages are *not* significantly different is represented by the intersection of these two probabilities, i.e. $(0.4729)^2 = 0.224$. Therefore the probability that the ages are *distinct* is $1.000 - 0.224 = 0.776$. Thus the ages are distinct at a confidence level less than 77.6%, but are not significantly different at a confidence level greater than 77.6%. Using the method outlined above, the exact 'distinguishability' confidence levels for all three age pairs were calculated, and these are summarised below Fig. 10. The probability that *all three* ages are distinct is the cumulative probability of these 'distinguishability' confidence levels. The final result (65.9%) suggests that overall it is reasonably likely that the three ages are all distinct from each other. In contrast, the probability that the ages are all the same is approximately 2%.

The high probability that plutonism and deformation took place over an interval longer than that required for conductive cooling and solidification of the magmas is strongly supported by the field relationships presented in the previous section. The existence of a uniform intrusion sequence of compositionally distinct magmas, and deformation events which display consistent cross-cutting relationships both with each other and within the intrusive chronology, together suggest that regional D_3 deformation and emplacement of the Mabel Downs Tonalite was protracted and comprised a discrete sequence of magmatic and deformational episodes. In comparison, if the total duration of magmatism and deformation was short (e.g. less than one million years), the considerable scope for temporal overlap both between individual intrusive episodes and between magmatism and locally recognised deformation events should have resulted in widespread mutual cross-cutting relationships between intrusive phases and an inconsistent relative deformation chronology, neither of which was observed in the studied outcrops.

5. Duration of intrusion and deformation

The integrated field, microstructural and geochronological data presented above suggest that the interval over which magmatism took place spanned the two locally recognised deformation events. Firstly, despite the large errors at the 95% confidence level associated with the pooled SHRIMP ages presented in the previous section, there is a consistent relationship between $^{207}Pb/^{206}Pb$ zircon ages and the position of the host granitoid in the deformation chronology. The presence of a strong tectonic S_{3a} foliation in the 1837.3 ± 6.0 Ma porphyritic monzogranite MD-1, a corresponding but weaker S_{3a} fabric in the 1831.9 ± 3.3 Ma granodiorite MD-2, and the absence of solid-state deformation in the 1826.6 ± 7.3 Ma microgranodiorite vein MD-3 collectively suggest that the intrusive phases bracket at least one episode of solid-state deformation. Secondly, the constant position of the majority of rock types within the relative deformation chronology in the Spring Creek outcrops suggests that the field relationships observed are the product of several discrete and distinguishable episodes of deformation and magmatism. Magmas emplaced as a single 'batch' during deformation commonly display an extensive range of mutual cross-cutting relationships both between intrusive phases and between magmatism and overprinting deformation (Vernon et al., 1988; D'Lemos et al., 1992; Karlstrom et al., 1993; McCaffrey et al., 1999). The absence of more widespread mutual cross-cutting relations between *all* phases in the Spring Creek outcrops suggests that Mabel Downs plutonism spanned a longer interval than that required to simply cool the interacting magmas below their respective solidi.

The interaction between local deformation and the three dated intrusives also imposes important constraints on the detail of the chronology. For example, the difference in intensity of the S_{3a} foliation in monzogranite MD-1 and granodiorite MD-2 (both of which pre-date D_{3b}) can be explained by (i) a real age difference between the two intrusive phases (i.e. igneous crystallisation of MD-2 at 1831.9 ± 3.3 Ma occurred during the waning stages of the D_{3a} deformation recorded by MD-1 at 1837.3 ± 6.0 Ma); (ii) differences in the intensity of deformation affecting the granitoids, possibly as a function of either distance from the pluton margin or pre-existing igneous textures, since it is possible that the coarse-grained porphyritic texture of monzogranite MD-1 accentuated the effects of subsequent solid-state deformation. Fig. 11 shows the two possible schematic relationships between the three Mabel Downs intrusives and progressive D_3, within the regional deformation framework.

We prefer (i) on the basis of the similarity in structural level of the Spring Creek outcrops (containing MD-2 and MD-3) and the location of monzogranite MD-1, both of which were very close to the structural base of the Mabel Downs Tonalite prior to the development of S_{3b} shear zones, intrusion of microdiorite dykes and F_4 folding. As the intensity of D_{3a} deformation increases towards the pluton margins elsewhere in the Mabel Downs Tonalite, monzogranite MD-1 and granodiorite MD-2 should have had similar responses to D_{3a} tectonism if both intrusives pre-dated the deformation event. Instead, granodiorite MD-2 preserves traces of a magmatic foliation that is no longer apparent in porphyritic monzogranite MD-1. As a result, we contend that there is an age difference between MD-1 and MD-2, and that the intrusives bracket the peak of regional D_{3a} deformation. Intrusion of granodiorite MD-2 during the waning stages of D_{3a} would account for the observed overprinting of a primary magmatic foliation by a tectonic fabric.

5.1. Position of D_3 and the Mabel Downs Tonalite in the regional thermal history

The D_{3b} event is clearly bracketed by MD-2 and MD-3 (Fig. 5), therefore granodiorite MD-2 is late- to post-D_{3a} and pre-D_{3b}, and its U–Pb SHRIMP zircon age of 1831.9 ± 3.3 Ma is the best estimate of the timing of regional D_3 east of the S_4 Highway Shear Zone, which represents a metamorphic discontinuity. This relationship is important in terms of the temperature–time path for the mid-crustal section currently exposed in the northern Central zone (Fig. 1b). Peak metamorphism in the Tickalara Metamorphics occurred at ~1845 Ma on both sides of the Highway Shear Zone (Oliver et al., 1999; Bodorkos et al., 2000). To the west of the Highway Shear Zone, the post-peak metamorphic Sally Malay layered mafic intrusion (U–Pb SHRIMP zircon age 1841 ± 3 Ma; Trudu and Hoatson, 1996) displays intrusive relationships and textures consistent with its emplacement into metapelites that were already hot (Oliver and Barr, 1997). The earliest phases of the Mabel Downs Tonalite rapidly followed (within 10 million years) on the eastern side of the Highway Shear Zone, but intrusive relationships are consistent with emplacement into lower-temperature host rocks (Bodorkos et al., 1999). However, pressure estimates from thermobarometric data in the vicinity of the two intrusions give similar values (~400 MPa; Thornett, 1986; Magart, 1994), suggesting that despite differences in peak metamorphic temperatures, the areas separated by the Highway Shear Zone were at approximately the same mid-crustal level prior to their juxtaposition during D_4 (Fig. 1b).

An external constraint on the cessation of regional D_3 east of the Highway Shear Zone is provided by the nearby Sally Downs Tonalite, which has a U–Pb SHRIMP zircon age of 1821 ± 4 Ma (Sheppard et al., 1995). This post-D_3 pluton contains a weak magmatic foliation and preserves no evidence of solid-state ductile deformation. Foliations in rocks on both sides of

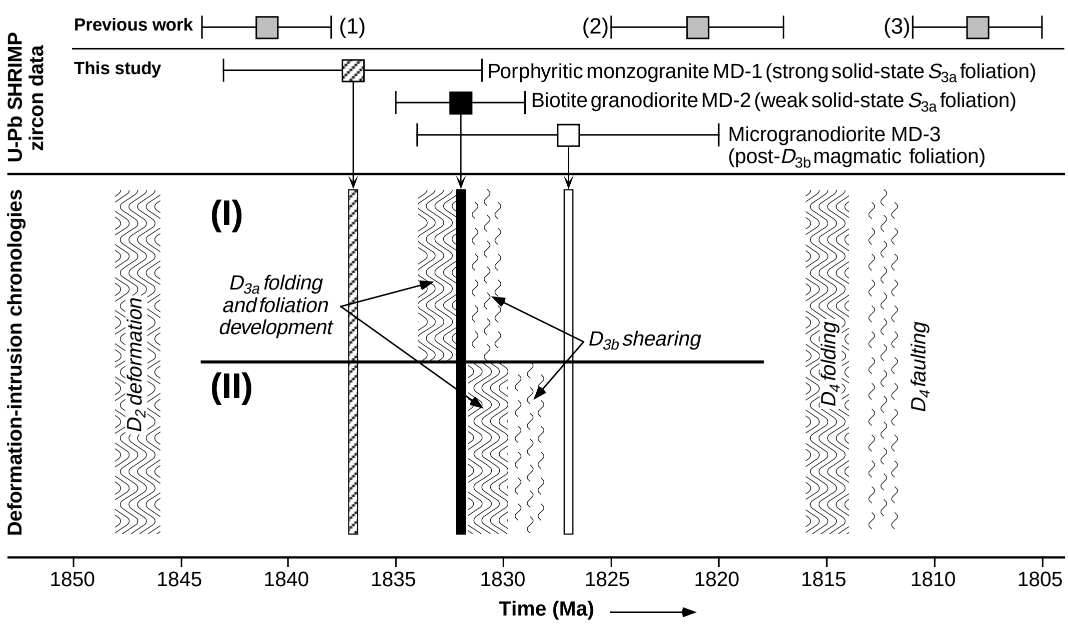

Fig. 11. Diagram showing possible relationships between the dated intrusive phases of the Mabel Downs Tonalite and the D_3 event, within the regional deformation chronology. Note that in the alternative chronologies (I) and (II), the absolute timing of individual intrusion crystallisation has been held constant, for simplicity in depicting their relationships to the D_3 event. In chronology (I), granodiorite MD-2 intrudes during the waning stages of D_{3a} deformation, and differences in the intensity of the S_{3a} foliation in MD-1 and MD-2 can be explained in terms of a real age difference between the intrusives. In chronology (II), MD-1 and MD-2 are both pre-D_3, and differences in the effect of D_{3a} on these two samples are ascribed to pluton-scale strain heterogeneities and/or the effect of pre-existing igneous textures. U–Pb SHRIMP zircon data providing constraints on regional D_2 and D_4: (1) = post-F_2 Sally Malay layered mafic intrusion, 1841 ± 3 Ma (Trudu and Hoatson, 1996); (2) = post-D_3 and pre-F_4 Sally Downs Tonalite, 1821 ± 4 Ma (Sheppard et al., 1995); (3) = post-F_4 Mount Christine Granitoid, 1808 ± 3 Ma (Sheppard et al., 1995).

the Highway Shear Zone are folded around a tight NNE-trending macroscopic F_4 antiform, the limbs of which are truncated by kilometre-scale brittle fault zones parallel to F_4 axial traces. One of these faults is stitched by an ~1810 Ma granitoid in the southern Halls Creek Orogen (Sheppard et al., 1995), which provides a younger age limit for D_4 deformation.

6. Implications for the interpretation of syn-plutonic deformation events

Many studies of the interaction between deformation and plutonism utilise comparisons of estimated crustal strain rates during orogenesis with approximate duration of pluton solidification processes. Simple thermal modelling of the cooling by conduction of tabular granite-like bodies emplaced in the middle crust (where the temperature contrast between the liquid magma and the host rocks is unlikely to be significantly greater than 500°C) suggests that pluton crystallisation occurs very rapidly, even for intrusive sheets of kilometre-scale thickness. Karlstrom et al. (1993) applied the equations of Turcotte and Schubert (1982) to the cooling of the Cretaceous East Piute pluton in southeastern California, a 3–4-km-thick granodiorite sheet (estimated solidus temperature ~750°C) emplaced into host rocks at a temperature of 300°C. A *maximum* crystallisation time of $\sim 10^5$ y was obtained.

These data can be used in conjunction with studies of accumulated finite strain in a large number of Phanerozoic orogenic belts (summarised by Pfiffner and Ramsay, 1982) in order to infer crustal strain rates during syn-plutonic deformation. Pfiffner and Ramsay (1982) suggested that the build-up (by steady-state flow) of geologically moderate finite strains over time intervals less than ~5 million years necessitates average strain rates in the range 10^{-13}–10^{-15} s^{-1}. Strain rates in excess of 10^{-13} s^{-1} produce very high strains, or require an extremely short deformation event ($= 10^4$ y; Pfiffner and Ramsay, 1982). Based on major- and trace-element geochemistry, Karlstrom et al. (1993) argued that the East Piute pluton represents a single 'batch' of magma within which chemical variations between distinguishable intrusive phases are attributable to fractional crystallisation processes. As a result, the duration of crystallisation precisely defines the time interval in which fabric development took place, based on shear strain estimates from latest syn-tectonic felsic dykes emplaced in tension gashes when the pluton was nearly completely crystallised (Karlstrom et al., 1993). As a result, producing the moderate amount of strain observable in the East Piute pluton within $\sim 10^5$ y requires a very high orogenic strain rate of 10^{-11}–10^{-12} s^{-1}; such rates may be possible in the case of short-lived localised episodic events assisted by melt-enhanced deformation (Hollister and Crawford, 1986; Karlstrom et al., 1993).

The Mabel Downs Tonalite approximates a tabular body of similar thickness to the Cretaceous East Piute pluton described by Karlstrom et al. (1993). Comparatively, the mafic composition and the scarcity of inherited zircon in the Mabel Downs Tonalite probably indicates a higher mean solidus temperature [~800°C, using the Zr saturation calculations of Watson and Harrison (1983) and assuming $>95\%$ of the Zr concentration measured in the granite was required for Zr-saturation of the magma]. However, this is balanced by the likelihood of higher host-rock temperatures (>400°C) during its emplacement. Pluton solidification times derived from the equations of Turcotte and Schubert (1982) depend principally on the thickness of the intrusion and the magma–host rock temperature *contrast* (rather than the temperature values themselves), and these two parameters are very similar for the East Piute pluton and the Mabel Downs Tonalite. Therefore we suggest that the granitoids of the Mabel Downs Tonalite crystallised within $\sim 10^5$ y of emplacement, with the important proviso that they comprise a single, instantaneously emplaced igneous body.

However, an important difference between the East Piute pluton and the syn-magmatic deformation of the Mabel Downs Tonalite involves the possibility of episodic emplacement of the intrusion. Emplacement of voluminous mingled microdiorite magma into pre-existing, substantially crystallised granitoids in the vicinity of the Ord River Shear Zone constitutes at least circumstantial field evidence that the Mabel Downs Tonalite was not intruded as a single magmatic pulse. Furthermore, preliminary Sr isotopic data suggest that the range of granitoid compositions were not derived by chemical differentiation of a single source (S. Bodorkos and A.A. Nemchin, unpublished data). In this case, 'syn-tectonic' deformation is not restricted to the pluton solidification interval of a single igneous body, and it is likely that real (if not resolvable) age differences between intrusive phases are comparable to the duration of intervening deformation events. This suggests that anomalously high orogenic strain rates over short time intervals are *not* required in order to produce the observed deformation features in the Mabel Downs Tonalite and its host rocks. The moderate degree of shear strain observed may equally be the result of lower crustal strain rates over a longer period of time. This is consistent with the development of D_3 structures on a regional scale and the constraints imposed by the U–Pb SHRIMP zircon data.

The prolonged nature of D_3 deformation at ~1830 Ma, when combined with evidence for a protracted thermal event in the Halls Creek Orogen (during which mid-crustal temperatures remained above ~400–

500°C in the interval ~1850–1820 Ma; Bodorkos et al., 1999) is significant in terms of the pattern of finite strain accumulation during orogenesis. The relatively rapid succession of three recognisable, macroscopic deformation events D_2, D_3 and D_4 (all of which occurred in the interval ~1850–1810 Ma) imply that individual deformation phases did *not* sharply punctuate periods of quiescence in a long-lived orogeny, but were each of moderately long duration (of the order of a few million years). As a result, strain may have accumulated at moderate to low rates regionally, in contrast with other orogenic belts where evidence exists for either higher shear strains or longer 'intradeformational lulls' (e.g. Bell, 1981; Tobisch and Paterson, 1990).

7. Conclusions

The combined field, petrological and geochronological data presented here suggest that intrusion of the Mabel Downs Tonalite involved protracted and repeated magmatism, spanning D_3 deformation in the central Halls Creek Orogen. Despite large errors at the 95% confidence level on the U–Pb SHRIMP zircon ages, the high probability of distinguishable differences in ages between intrusive phases is significant in the context of studies of syn-tectonic plutonism which seek to constrain the *duration* of episodic deformation with respect to intrusion in order to infer local orogenic strain rates (e.g. Karlstrom et al., 1993; McCaffrey et al., 1999). Pluton solidification processes in the upper- and middle-crust are demonstrably rapid even for large bodies; however, the timing of associated deformation can only be broadly constrained, even when extremely precise geochronological data are available. In addition, evidence for episodic magmatism and/or multiple magma sources (on the basis of field relations, geochemical or isotopic evidence) severely complicates calculations of a proposed duration for pluton-scale deformation. We therefore advocate caution in the inference of orogenic strain rates based on the duration of syn-tectonic deformation of a crystallising pluton, especially when the interacting pluton is the product of two or more discrete magmatic episodes, which may be separated in time by intervals that exceed the proposed duration of the deformation event, based on the solidification time of a single, instantaneously emplaced batch of magma.

Acknowledgements

This work was carried out while SB was in receipt of a Curtin University Postgraduate Scholarship. The research was funded by Australian Research Council Large Grant no. C39702277 awarded to NHSO. We thank Steve Sheppard and Ian Tyler for informative and constructive discussions, and Daniel Clark and Robin Rennie for assistance in the field. Critical and constructive reviews by Andy Tulloch, Martin Hand and Richard Norris resulted in substantial improvements to the manuscript. Gerhard Vavra generously provided access to unpublished data. This is Tectonics Special Research Centre Publication No. 106.

References

Bell, T.H., 1981. Foliation development—the contribution, geometry and significance of progressive, bulk, inhomogeneous shortening. Tectonophysics 75, 273–296.

Bodorkos, S., Cawood, P.A., Oliver, N.H.S., 1998. Temperature–time (T–t) path for the Tickalara Metamorphics of the Halls Creek Orogen, W.A.: implications for tectonic models. Geological Society of Australia Abstracts 50, 8–10.

Bodorkos, S., Cawood, P.A., Oliver, N.H.S., Nemchin, A.A., 2000. Rapidity of orogenesis in the Palaeoproterozoic Halls Creek Orogen, northern Australia: evidence from SHRIMP zircon data, CL zircon images and mixture modeling studies. American Journal of Science 300, 60–82.

Bodorkos, S., Oliver, N.H.S., Cawood, P.A., 1999. Thermal evolution of the central Halls Creek Orogen, northern Australia. Australian Journal of Earth Sciences 46, 453–465.

Brown, M., Solar, G.S., 1998. Shear-zone systems and melts: feedback relations and self-organization in orogenic belts. Journal of Structural Geology 20, 211–227.

Buddington, A.F., 1959. Granite emplacement with special reference to North America. Geological Society of America Bulletin 70, 671–747.

Castro, A., 1986. Structural pattern and ascent model in the Central Extremadura batholith Hercynian belt, Spain. Journal of Structural Geology 8, 633–645.

D'Lemos, R.S., Brown, M., Strachan, R.A., 1992. Granite magma generation, ascent and emplacement within a transpressional orogen. Journal of the Geological Society of London 149, 487–490.

Gower, C.F., 1993. Syntectonic minor intrusions or synemplacement deformation? Canadian Journal of Earth Sciences 30, 1674–1675.

Griffin, T.J., Tyler, I.M., 1992. Geology of the southern Halls Creek Orogen—a summary of field work in 1992. In: Geological Survey of Western Australia Record, 1992/17.

Hollister, L.S., Crawford, M.L., 1986. Melt-enhanced deformation: a major tectonic process. Geology 14, 558–561.

Hutton, D.H.W., 1988. Granite emplacement mechanisms and tectonic controls: inferences from deformation studies. Transactions of the Royal Society of Edinburgh: Earth Sciences 79, 245–255.

Karlstrom, K.E., 1989. Towards a syntectonic paradigm for granitoids. EOS, Transactions of the American Geophysical Union 70, 762–764.

Karlstrom, K.E., Miller, C.F., Kingsbury, J.A., Wooden, J.L., 1993. Pluton emplacement along an active ductile thrust zone, Piute Mountains, southeastern California: interaction between deformation and solidification processes. Geological Society of America Bulletin 105, 213–230.

Kendrick, T., Rey, P., Costa, S., Masur, G., Foley, B., 1999. Synchronous transpression and magmatism in the Halls Creek Mobile Belt (East Kimberley, WA). Geological Society of Australia Abstracts 53, 131–133.

Magart, A.P.M., 1994. A metamorphic and metasomatic study of marbles and calc–silicate rocks within the Tickalara

Metamorphics, east Kimberley region, Western Australia. BSc(Hons) thesis, Monash University, Melbourne, Australia.

McCaffrey, K.J.W., Miller, C.F., Karlstrom, K., Simpson, C., 1999. Synmagmatic deformation patterns in the Old Woman Mountains, SE California. Journal of Structural Geology 21, 335–349.

Nelson, D.R., 1997. Compilation of SHRIMP U–Pb zircon geochronology data, 1996. Geological Survey of Western Australia Record 1997/2, 189 p.

Oliver, N.H.S., Barr, T.D., 1997. The geometry and evolution of magma pathways through migmatites of the Halls Creek Orogen, Western Australia. Mineralogical Magazine 61, 3–14.

Oliver, N.H.S., Bodorkos, S., Nemchin, A.A., Kinny, P.D., Watt, G.R., 1999. Relationships between zircon U–Pb SHRIMP ages and leucosome type in migmatites of the Halls Creek Orogen, Western Australia. Journal of Petrology 40, 1553–1575.

Oliver, N.H.S., Valenta, R.K., Wall, V.J., 1990. The effect of heterogeneous stress and strain on metamorphic fluid flow, Mary Kathleen, Australia, and a model for large scale fluid circulation. Journal of Metamorphic Geology 8, 311–331.

Page, R.W., Sun, S., 1994. Evolution of the Kimberley region, W.A. and adjacent Proterozoic inliers—new geochronological constraints. Geological Society of Australia Abstracts 37, 332–333.

Page, R.W., Hoatson, D.M., Sun, S., Foudoulis, C., 1995a. High-precision geochronology of Palaeoproterozoic layered mafic–ultramafic intrusions in the East Kimberley. AGSO Research Newsletter 22, 7–8.

Page, R.W., Tyler, I.M., Blake, D.H., 1995b. Geochronology of magmatism and high-grade metamorphism, Kimberley region. W.A. Australian Conference on Geochronology and Isotope Geoscience Abstracts 3, Curtin University, Perth, p. 25.

Paterson, S.R., 1989. Are syntectonic granites truly syntectonic? EOS, Transactions of the American Geophysical Union 70, 764–765.

Paterson, S.R., Vernon, R.H., Tobisch, O.T., 1989. A review of criteria for the identification of magmatic and tectonic foliations in granitoids. Journal of Structural Geology 11, 349–363.

Pearson, P.J., Holcombe, R.J., Page, R.W., 1992. Synkinematic emplacement of the Middle Proterozoic Wonga Batholith into a mid-crustal extensional shear zone, Mount Isa Inlier, Queensland, Australia. In: Stewart, A.J., Blake, D.H. (Eds.), Detailed Studies of the Mount Isa Inlier, Australian Geological Survey Organisation Bulletin, 243. Australian Geological Survey Organisation, Canberra, Australia, pp. 289–328.

Pfiffner, O.A., Ramsay, J.G., 1982. Constraints on geological strain rates: arguments from finite strain states of naturally deformed rocks. Journal of Geophysical Research 87, 311–321.

Sheppard, S., Griffin, T.J., Tyler, I.M., 1995. Geochemistry of felsic igneous rocks from the southern Halls Creek Orogen. In: Geological Survey of Western Australia Record 1995/4, 81 p.

Sheppard, S., Griffin, T.J., Tyler, I.M., 1997. The tectonic setting of granites in the Halls Creek and King Leopold Orogens, northwest Australia. In: Rutland, R.W.R., Drummond, B.J. (Eds.), Palaeoproterozoic Tectonics and Metallogenesis: Comparative analysis of parts of the Australian and Fennoscandian Shields, AGSO Record, 1997/44. Australian Geological Survey Organisation, Canberra, Australia, pp. 107–109.

Sheppard, S., Tyler, I.M., Griffin, T.J., Taylor, W.R., 1999. Palaeoproterozoic subduction-related and passive margin basalts in the Halls Creek Orogen, northwest Australia. Australian Journal of Earth Sciences 46, 679–690.

Solar, G.S., Pressley, R.A., Brown, M., Tucker, R.D., 1998. Granite ascent in convergent orogenic belts: testing a model. Geology 26, 711–714.

Thornett, J.R., 1986. Evolution of a high-grade metamorphic terrain in the Proterozoic Halls Creek Mobile Zone, Western Australia. PhD thesis, University of Western Australia.

Tobisch, O.T., Paterson, S.R., 1990. The Yarra granite: an intradeformational pluton associated with ductile thrusting, Lachlan Fold Belt, southeastern Australia. Geological Society of America Bulletin 102, 693–703.

Trudu, A., Hoatson, D.M., 1996. Depths of emplacement of Precambrian layered intrusions in the East Kimberley. AGSO Research Newsletter 25, 10–12.

Turcotte, D.L., Schubert, G., 1982. Geodynamics: Applications of continuum physics to geological problems. John Wiley & Sons, New York.

Tyler, I.M., Griffin, T.J., Page, R.W., Shaw, R.D., 1995. Are there terranes within the Lamboo Complex of the Halls Creek Orogen? Geological Survey of Western Australia Annual Review 1993/94, 37–46.

Tyler, I.M., Page, R.W., Griffin, T.M., 1999. Depositional age and provenance of the Marboo Formation from SHRIMP U–Pb zircon geochronology: Implications for the early Palaeoproterozoic tectonic evolution of the Kimberley region, Western Australia. Precambrian Research 95, 225–243.

Vernon, R.H., 1991. Questions about myrmekite in deformed rocks. Journal of Structural Geology 13, 979–985.

Vernon, R.H., Etheridge, M.A., Wall, V.J., 1988. Shape and microstructure of microgranitoid enclaves: indicators of magma mingling and flow. Lithos 22, 1–11.

Watson, E.B., Harrison, T.M., 1983. Zircon saturation revisited: temperature and composition effects in a variety of crustal magma types. Earth and Planetary Science Letters 64, 295–304.